Calcite-functionalized micromodels for pore-scale investigations of CO₂ storage security

Malin Haugen[1,*], *Benyamine* Benali[1], *Tore* Føyen[1, 2], *Wen* Song[3], *Martin* A. Fernø[1], and *Bergit* Brattekås[1]

[1]Department of Physics and Technology, University of Bergen, Norway
[2]SINTEF Industry, Norway
[3]Hildebrand Department of Petroleum and Geosystems Engineering, University of Texas at Austin, USA

Abstract. Carbon capture and subsequent storage (CCS) is identified as a necessity to achieve climate commitments. Permanent storage of carbon dioxide (CO₂) in subsurface saline aquifers or depleted oil and gas reservoirs is feasible, but large-scale implementation of such storage has so far been slow. Although sandstone formations are currently most viable for CO₂ sequestration, carbonates play an important role in widespread implementation of CCS; both due to the world-wide abundancy of saline aquifers in carbonate formations, and as candidates for CO₂-EOR with combined storage. Acidification of formation brine during CO₂ injection cause carbonate dissolution and development of reactive flow patterns. Using calcite-functionalization of micromodels we experimentally investigate fundamental pore-scale reactive transport dynamics relevant for carbonate CO₂ storage security. Calcite-functionalized, two-dimensional and silicon-based, pore scale micromodels were used. Calcite precipitation was microbially induced from the bacteria *Sporosarcina pasteurii* and calcite grains were formed *in-situ*. This paper details an improved procedure for achieving controlled calcite precipitation in the pore space and characterizes the precipitation/mineralization process. The experimental setup featured a temperature-controlled micromodel holder attached to an automatic scanning stage. A high-resolution microscope enabled full-model (22x27 mm) image capture at resolution of 1.1 μm/pixel within 82 seconds. An in-house developed image-analysis python script was used to quantify porosity alterations due to calcite precipitation. The calcite-functionalized micromodels were found to replicate natural carbonate pore geometry and chemistry, and thus may be used to quantify calcite dissolution and reactive flow at the pore-scale.

1 Introduction

Commitments to reach climate goals require us to reduce greenhouse gas concentrations in the atmosphere. Carbon capture, utilization, and storage (CCUS) is identified to play a critical role in achieving these goals. In the Clean Technology Scenario presented by IEA, CCUS is the third-largest contributor (13%) to the cumulative emission reduction until 2060 [1]. Among other, CO₂ can be stored in deep saline aquifers within sandstone or carbonate formations. However, two of the possible risk aspects related to CO₂ storage is the potential for leakage to the surface and, for carbonate formations, dissolution of the reactive calcite rock minerals. The storage potential in carbonate reservoirs is large, but the reactive transport and mechanisms must be accounted for.

Biomineralization is the formation of minerals by living organisms. Microbial induced calcite precipitation (MICP) has been researched in conjunction with different engineering applications, for instance within construction engineering to seal fracture or strengthen concrete [2], for enhanced oil recovery [3, 4], to constrain contaminated groundwater [5], for cementation of unconsolidated porous media [6], and for CO₂ sequestration by reduction of permeability in fractured rock to potential seal leakage paths in the near well area and/or in the cap-rock [7-9].

Precipitation of calcium carbonate (CaCO₃) is controlled by four key factors: (1) concentration of calcium (Ca^{2+}) from the cementation solution, (2) concentration of dissolved inorganic carbon as produced by ureolysis, see equation 1-5 in section 2.2, (3) pH value, and (4) availability of nucleation sites [10]. CaCO₃ precipitation is dependent on presence of sufficient calcium and carbonate ions to ensure that the ion activity product exceed the solubility product, making the system oversaturated and precipitation of calcium carbonate is likely. Microbial metabolic activity influence key factor no. 2 and 3, and also no. 4 by function as nucleation site [2]. Calcium carbonate is a common element found in many rocks, such as chalk and marble, it is also the main component in shells, pearls, and corals. CaCO₃ can crystallize in different polymorphs, seen as minerals in the nature. This includes calcite, vaterite and aragonite, with calcite as the most stable, and two hydrated polymorphs in addition to several amorphous phases (ACC) [11]. Vaterite is the least thermodynamically stable polymorph and transforms rapidly to calcite or aragonite in aqueous solutions. According to Ostwald's rule of stages, metastable polymorphs are first formed and then transform into thermodynamically more stable polymorphs [12]. For high supersaturation values it is reported that calcite is initially precipitated as the hydrous form of ACC (tens to hundreds of nanometer) which are subsequently transformed into spherical vaterite and later calcite, while lower supersaturation values lead to direct calcite precipitation [13, 14].

A bacteria often used for studying of MICP in the laboratory is the soil bacteria *Sporosarcina pasteurii* [3, 15-18]. In this research this bacteria have also been utilized, with the goal to build upon work by Song et al. 2018 [18] and present an improved procedure to functionalize the pore space in a micromodel with CaCO₃ and enable recording of continuous full-model images. A micromodel is a device with a porous pattern from a representative rock matrix etched into a silicon wafer

before an optical transparent glass plate is bonded on top. It has four fluid flow ports, one in each corner, with an open fracture connecting two pairs of flow ports (Fig.). This device enable direct study of microscale interactions between fluids and rocks. By functionalizing micromodels with an existing pore-network made of silica grains, it is possible to both precipitate and dissolve $CaCO_3$ minerals and still re-use the micromodel afterwards. This starting point is therefore of great interest during study of fundamental pore-level reactive transport dynamics that determine CO_2 storage security in carbonate formations. MICP in micromodels have also been studied by Wang [19, 20], where, among other, the effect of bacterial cells was studied as well as evolution of shape and size of the $CaCO_3$ precipitates during the MICP process. In this paper we are adding quantification of change in porosity due to $CaCO_3$ precipitation and pressure development throughout experiments.

The experimental set-up was designed to facilitate flow experiments at pressures between 0-120 bars and temperatures between 25-40 °C. Because of the dependency on the biological process, it is important to regulate the temperature to adjust the growth rate of the bacteria. Further, the tubing and valves included in the set-up provide a low, constant, dead volume. The possibility of independent injection and production from each of the four ports in the micromodel, combined with injection of bacterial solution through a loop with constant volume provide excellent experimental conditions. The result is a permeable porous model with carbonate grains distributed throughout the whole pore volume.

By utilizing an in-house built program, we can calculate change in porosity, and among other, identify area of representative elementary volume. The utilized microscope has an automatic scanning stage and a fluorescence module, which enable us to capture the complete porous network (22x27 mm) with resolution of 1.1 μm/pixel. This paper starts with an overview of the micromodel and bacteria utilized to functionalize the micromodel with calcium carbonate. Then, the experimental set-up and equipment is described, followed by the experimental procedures. Results in the form of images, porosity development due to in-situ $CaCO_3$ precipitation and relevance to CO_2 sequestration are presented, before concluding remarks.

2   Materials and methods
2.1   Micromodel

Direct study of microscale interactions between fluids and rocks at elevated reservoir temperature and pressure were enabled by microfluidic devices, further referred to as micromodels. The micromodels consist of two parts, an optical transparent borosilicate glass plate bonded on top of a silicon wafer with etched pattern of a representative porous rock matrix. The state-of-the-art etching method provides a two-dimensional porous system with representative pore-scale geometry with vertical grain walls, sharp edges, and a hydrophilic surface.

The porous network is based on thin sections from natural sandstone, a rock type widely used in laboratory flow experiments for enhanced oil recovery and/or CO_2

storage. Dead-end and isolated pores in the thin section were modified in the micromodel to enable flow across the whole pattern, resulting in higher micromodel porosity and permeability compared to the natural sandstone sample. A unique porous network (6.74 x 2.50 mm) was extracted from the thin section and etched in the silicon wafer with a constant depth of 30 μm. The unique pore pattern was repeated 36 times (4 x 9), resulting in a total porous network which is 27.0 x 22.5 mm large (Fig. **1**). The grains are discontinuous and irregularly shaped, providing flow tortuosity. In each corner, a port through the silicon wafer can connect the pore network to external fluid flow tubes. Two open channels between ports improve flow communication and sweep of the pore space. Further details about design and production procedures can be found in [21] and [22].
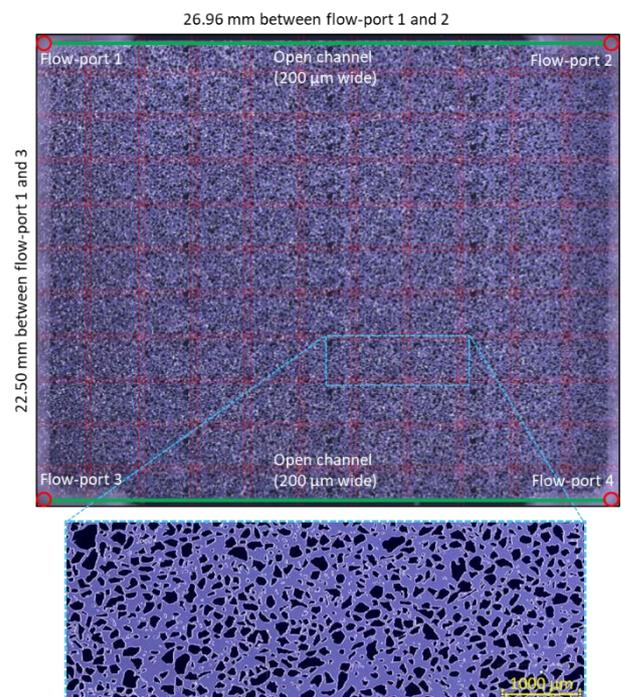
Fig. 1. Full-model image of a micromodel including dimensions. The four flow-ports and the two open-channel fractures between two pairs of ports are highlighted. A pattern generated from thin sections of natural sandstone is repeated 36 times to create the micromodel porous network. A zoom-in of the repeated pattern is highlighted in blue. The full-model image is generated from 121 individual images automatically captured by the microscope software with 10% overlap (shown in red dotted lines), stitched together to one image.

Micromodel properties are listed in Table **1**, as previously reported by Benali et.al (2021) [23]. Stitched full-model images were analyzed to determine grain size distribution, pore throat length distribution (defined as the shortest pore space distance between two neighboring grains) and porosity. Porosity was quantified to 0.61 based on amount of pore space to the total area (grains + pore space) and the total micromodel pore volume (PV) was 11.1 μL. Fig. **2** shows the distribution of grains and pore throat length in the micromodel. Average grain size is calculated to 6 464 μm^2 and average pore throat length is 41 μm, with the shortest pore throat being 0.7 μm with square or rectangular cross-section.

Table 1. Micromodel properties

Parameter	Value
Width	27.0 mm
Length	21.4 mm
Depth	30 μm
Porosity	0.61
Pore volume	11.1 μL
Permeability	2.97 D
Repetition of pattern	36
Grain size	0.5 - 78 366 μm²
Pore throat length	0.7 - 194 μm
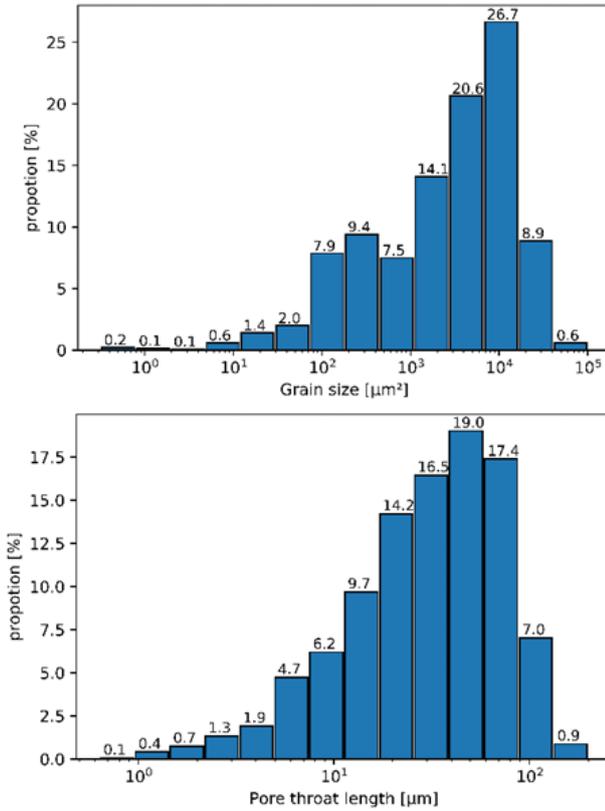
Fig. 2. Distribution of grain size (top) and pore throat length (bottom) in one of the 36 pore network repetitions which make up the micromodel.

The work presented here describes the experimental set-up and method to functionalize micromodels with calcium carbonate grains utilizing bacteria. This enables experimental investigations of fundamental pore-scale reactive transport dynamics in carbonate rocks.

2.2 Sporosarcina pasteurii bacteria

To functionalize micromodels with calcium carbonate for pore-scale investigations of CO_2 storage security, microbially induced calcite precipitation (MICP) by urea hydrolysis have been utilized. The bacteria *Sporosarcina pasteurii*, formerly *Bacillus pasteurii,* (Miquel 1889) DSM33 [24] are urease positive [25] and has a known ability to enable calcite precipitation [15] and growth on solid surfaces [2, 3]. The bacterial cells are gram positive,

motile and rod shaped with size in the range of 0.5-1.2 x 1.3-4.0 μm [25]. This is an aerobic bacteria with optimum growth temperature and pH of 30 ºC and 9, respectively [25].

The MICP process has been studied by several researchers and the following equations (Eq.1-5) have typically been used to describe this process [2, 7, 17, 26]. The bacteria hydrolyze urea ($CO(NH_2)_2$) into ammonia (NH_3) and carbonic acid (H_2CO_3), see Eq.1. In solution this leads to production of (OH^-) and accumulation of ammonium (NH_4^+). As a result of increasing (OH^-) concentration, the pH in the microenvironment is increasing (Eq. 2 and 3), and subsequently causes carbonic acid to be converted to bicarbonate (HCO_3^-) and further to carbonate ions (CO_3^{2-}) (Eq.4). When calcium ions (Ca^{2+}) are added to the solution, the increasing pH also leads to precipitation of calcium carbonate ($CaCO_3$) [3, 7] when the solution is supersaturated with calcium- and carbonate- ions (Eq.5). Precipitation of calcium carbonate can occur in the bulk phase, or on the bacteria cell wall because it is negatively charged and will therefore attract the positive charged calcium ions [2, 16]. If the bacterium is covered in calcium carbonate the cell will die as nutrient transfer is prevented [2, 26].

$$CO(NH_2)_2 + 2H_2O \xrightarrow{urease} 2NH_3 + H_2CO_3 \quad (1)$$

$$2NH_3 + 2H_2O \leftrightarrow 2NH_4^+ + 2OH^- \quad (2)$$

$$H_2CO_3 + 2OH^- \leftrightarrow HCO_3^- + H_2O + OH^- \quad (3)$$

$$HCO_3^- + H_2O + OH^- \leftrightarrow CO_3^{2-} + 2H_2O \quad (4)$$

$$Ca^{2+} + CO_3^{2-} \rightarrow CaCO_3(s) \quad (5)$$
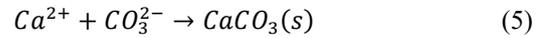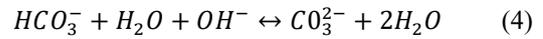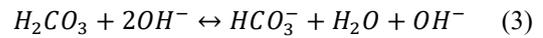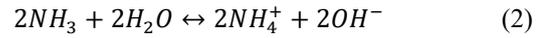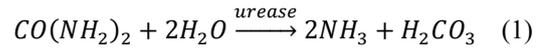
Details about preparing of bacteria and fluids, and procedure for functionalization of micromodels are described in section 2.4.

2.3 Experimental set-up

A schematic of the experimental set-up for *in situ* visualization of calcite-functionalized micromodels is presented in Fig. **3**. The system also contains equipment to inject CO_2 or CO_2-saturated fluids for pore-scale investigations of CO_2 storage security at elevated reservoir pressure and temperature (see section 3.3). To facilitate injection of these fluids, the set-up is designed with all tubes and equipment (except autoclave-valves) in materials which are chemical compatible with these fluids. Polyether ether ketone (PEEK) has been found to resist all the chemicals and fluids used in this work and is therefore the main material used in this design.

On the inlet side of the micromodel, a high precision plunger pump (Quizix 5000-2.5K) is operated in independent mode and used for injection of water and CO_2. There is also an option to inject CO_2 into an in-house PEEK accumulator (30 ml) for CO_2-saturated fluids. As mentioned in section 2.1, the smallest pore throat in the micromodel is calculated to be 0.7 μm. To avoid injection of unwanted particles, like dust, that clogs up the micromodel, all fluids were filtered prior to use and flow
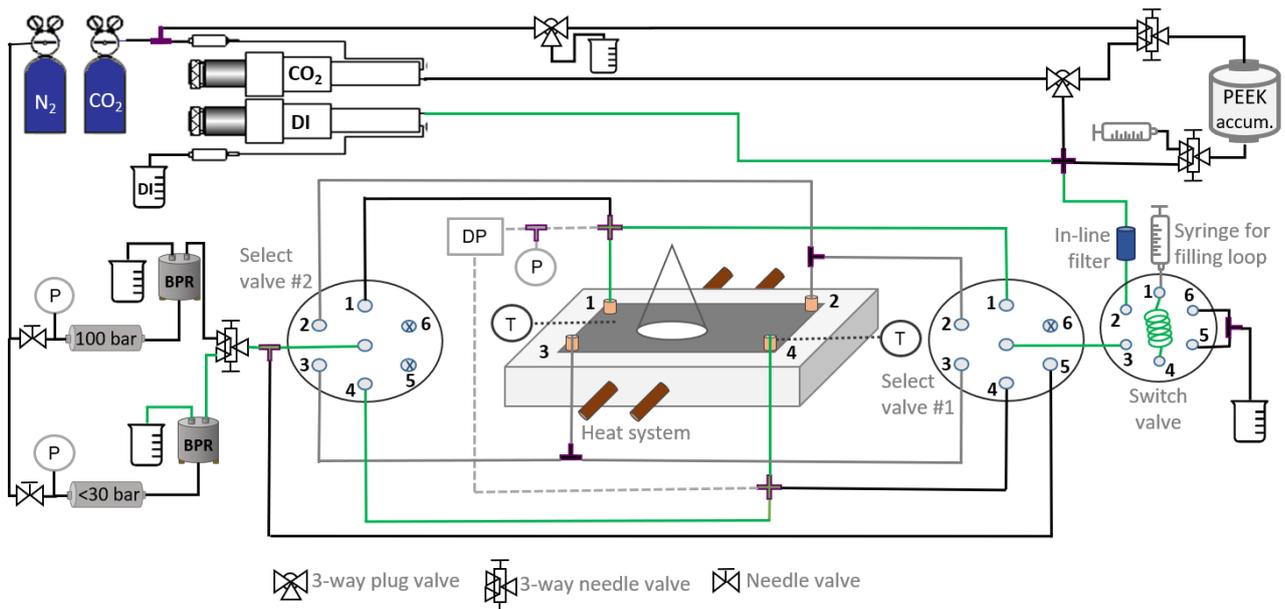
Fig. 3. Schematic of the experimental set-up for calcite-functionalization of micromodels. During injection of bacterial- or cementation solution, tubing marked in green were open/connected. Fluids were injected into a 1.0 ml loop in the switch valve and chased by DI from a pump. The micromodel was placed directly under a microscope, enabling in-situ visualization of $CaCO_3$ precipitation in the pore space. All tubing and tee/cross (purple) are in PEEK from Idex.

through a 0.5 μm inline filter assembly (Idex, A-431) prior to entering the micromodel.

The low pore volume (11.1 μL) makes it important to have a constant system dead-volume to ensure that fluids enter the micromodel when anticipated. This is achieved by utilizing two 6-ports select valves (Idex, MXP7970-000), one at inlet and one at the outlet. When valves #1 and #2 are connected to the fluid-flow-ports (Fig. **3**) it is possible to designate injection and production ports with a single mouse-click. When changing injection fluid, both select valves were set to position 5 for the fluids to by-pass the micromodel until pressure stabilized. During calcite generation experiments small amounts of different fluids will be injected into the model at various times. To facilitate variable fluid injection without air entering the tubes, a two-position switch valve (Idex, 9725) is included in the design. The switch valve has two positions: load and inject. At "load" position, fluids from the pump flow into port 2, via port 3 and to Select Valve #1. A coiled tube (referred to as "loop", see Fig 3) with a constant volume could then be filled with e.g. bacteria-solution using a luer-lock syringe. At "inject" position, flow from

the pump is rooted through the loop and into Select Valve #1. Other valves used in the set-up are Autoclave valves as described in Fig. **3**.

The system is pressurized by two back pressure regulators (Equilibar), where one is kept at 100 bars for high pressure experiments, and one at lower pressure depending on experimental design. The pressure differential between inlet and outlet is logged with differential pressure transmitter (APLISENS PRE-28 SMART) with a measuring range of 0-2.5 bar and a static pressure limit of 250 bar. In addition, absolute pressure transmitter (ESI), with range from 0-250 bar, is connected to flow port 1.

The micromodel-holder in the middle of Fig. **3** is designed and machined in-house from PEEK material. It consists of four drilled holes, made with a 10-32 coned drill, which is aligned with the fluid-flow-ports underneath the micromodel, two Omega temperature probes close to port number 1 and 4, and tracks for two 1/8-inch copper tubing for heating of the micromodel by circulation of warm water. Fluid flow tubes are connected to the micromodel-holder by finger tight fittings 10-32
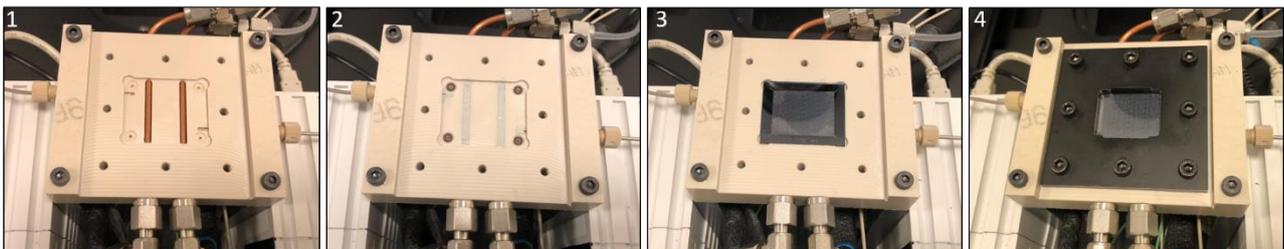
Fig. 4. Image sequence showing steps for mounting micromodel in holder. Left to right: The first image shows only the holder with machined groove for the micromodel, O-rings around the four fluid-flow-ports, two temperature gauges and copper tubing for the heating system. In the second image, the O-rings are in place and thermal paste are covering the temperature gauges and copper tubing to ensure optimal heat transfer. In the third image, the micromodel is in place and in the fourth image the black-painted aluminum plate is placed on-top of the micromodel and tightened with 0.20 Nm force. When everything is in place, the system can be pressurized to 150 bar.

coned (Idex, F-120X) screwed directly into the four drilled holes in the PEEK holder. Mounting of micromodel in the holder are shown in detail in Fig. **4**.

As indicated by the cone in Fig. **3**, the micromodel-holder is placed directly underneath a microscope to enable *in situ* visualization of calcite generation and subsequent investigation of CO_2 storage in carbonate formations. The microscope is a Zeiss, Axio Zoom.V16 Microscope including a Fluorescence module. It has an automatic scanning-stage which enables high-resolution imaging of the entire micromodel within 82 seconds (with the diffuser S light source) and automatic stitching of the images to a full-model image. When generating images with both diffuser S light source and one fluorescent (FL) light channel for each tile, a full-model image is acquired within 293 seconds.

2.4 Experimental procedure

2.4.1 Preparation of fluids

Bacterial growth medium and cementation solution (reactant) were prepared as described by [18]:

Bacterial growth medium: 47g of brain heart infusion broth (BHI Broth, 53286 Sigma-Aldrich) was mixed with 900 ml of deionized (DI) water, obtained from Milli-DI synthesis system including 0.2 µm filter (172-5109, Merck). Then the solution was sterilized in 15 minutes at 121 °C in an autoclave before cooled to ~30 °C. Next, a concentrated urea solution was added to make a 2 wt. % urea broth. This was achieved by mixing 20g of urea into 100 mL of DI water. Before injecting this urea solution into the growth medium, it was filtered through a 0.2 µm syringe filter (514-0061, VWR). The finished growth medium (BHI+U) was also filtered through the syringe filter prior to adding bacteria.

Reactant was prepared by mixing urea (urea, U5378, Sigma-Aldrich) and calcium chloride (calcium chloride dehydrate, 31306, Sigma-Aldrich) in DI water. As for the growth medium, the reactant was filtered through a 0.2 µm syringe filter prior to use to minimize the risk of small particles entering the micro-model.

2.4.2 Cultivation of bacteria

Bacterium *Sporosarcina pasteurii* DSM 33 [24] were received freeze-dried from DSMZ GmbH supplier and cultivated as follows: First the pellet was removed from the sealed glass and added to 0.5 ml growth medium where it was allowed to rehydrate for 30 minutes. Second, 0.2 ml of the bacterial solution was moved to a centrifuge tube containing 10 ml growth medium and placed in a heating cabinet at 30 ºC for 24 hours. Growth was detected after 24 hours, but the procedure was repeated one more time by adding 0.2 ml of the bacterial solution into a new centrifuge tube with 10 ml growth medium and stored in 30 ºC for another 24 hours. After 24 hours, sufficient bacterial growth was observed, and the bacterial solution was ready to be used. Every 7 days, 0.2 ml of bacterial solution is moved to a new centrifuge tube containing 10 ml growth medium to prevent death of bacteria. In case bacteria die, an inventory of glycerol stock was prepared by adding 0.2 ml of bacterial solution

and 0.2 ml of 30 % glycerol into 6 pendlorf microtubes for long term storage at -80 ºC.

2.4.3 Calcite-functionalization of micromodels

The experimental set-up (Fig. **3**) is designed to withstand pressure up to 150 bar, but the MICP process was performed at atmospheric pressure or slightly elevated pressure conditions (25 bars). The latter based on experience of when all CO_2 generated from the bacterial metabolism during settling time is completely dissolved in aqueous phase, to mitigate gas-filled pores that influence fluid flow. As the MICP process is developing to be utilized in more extreme environment [27], studying this process at elevated pressures is relevant. Several factors impact the precipitation of calcium carbonate during the MICP process and variables can be adjusted depending on the goal. Details about the experimental procedure used to generate calcium carbonate in a micromodel are explained below.

1. Initial conditions.
The micromodel is initially filled with deionized water (DI). DI is miscibly displaced by bacterial growth medium before 20 µl (2 PV) bacterial solution is injected at 6 µl/min (flow port 3 as inlet and 2 as outlet). 2 PV bacteria solution is consistent with results by Wang et.al (2018) [19], who have reported that bacterial suspension was homogeneously distributed in a microfluidic chip after 1.25 PV injected.

2. Bacterial growth in pore space.
Tubing used for bacterial solution are flushed with sterile bacterial growth medium before the micromodel is shut in. This enables time for bacteria to grow, settle and attach to the pore walls.

3. Prepare for injection of cementation solution.
Cementation solution is loaded in the loop of the switch valve and injected through the bypass next to flow port 1 (with both select-valves at position 1). When the bypass is filled with cementation solution, flow is routed at 1 µl/min to flow-port 1 in the micromodel, and flow port 2 is used as outlet.

4. Cementation solution into micromodel.
After the dead-volume from bypass to flow-port 1 has been injected, the outlet flow-port is changed from 2 to 4. *In situ* growth of calcium carbonate is visualized using a high-resolution microscope with automatic scanning stage, enabling full-model images of 1.1 µm/pixel within 82 seconds or 293 seconds if one FL channel is included.

2.5 Quantification of porosity

Changes in porosity from $CaCO_3$ precipitation were quantified from image analysis (using an in-house python script) on sub-sections during time-lapse imaging, and in the entire pattern for the last time step, see section 3.

Two different light sources (diffuser S and FL) were available for in-situ imaging of the micromodel, each with its own method for calculating the area of precipitated $CaCO_3$ minerals. With the diffuser S light source, calcium carbonate minerals appear white and can be quantified with simple segmentation. The white reflection edge around each silica grain were omitted from the areal

calculations by subtracting the initial image (experiment A). When both light sources were utilized, two approaches were developed, depending on when the FL tracer was injected: 1) displace the aqueous phase with a FL tracer after the MICP process. In the FL light image, the $CaCO_3$ minerals then appear as shades from green to black, where black minerals were interpreted as occupying the whole height in the micromodel; 2) include a FL tracer in the cementation solution during the MICP process. Calcite minerals then appear orange with the diffuser S light source (Fig.**6**, B.1). If the FL tracer is replaced with aqueous phase after the MICP process, only $CaCO_3$ minerals are visible in the FL light image. By combining threshold diffuser S and FL images, the result contains the area of all precipitated $CaCO_3$ (Experiment B).

Porosity changes over time can be studied by dividing the full-model images into sub-sections (experiment A). This is achieved by adding the total silica grain area to the calcium carbonate area for each timestep, then normalizing against initial white areas related to reflections around silica grains and bacterial aggregation or potential biofilm. With this approach we mitigate areas related to white reflections which otherwise would impact the porosity as the software/script identify all white colors as porosity. The final fraction of calcite minerals in the pore space was calculated as total calcite grains area divided by the total area of each image, both in the sub-sections and the full-model image. Some calcite grains (part of a whole grain) appear transparent and were not detected by the software. Hence, the calculated calcite fraction is expected to be lower than the real fraction.

3   Results and discussion

3.1   Experimental conditions

Two experiments, with the same bacterial culture and procedure, constitute the experimental results in this study. The pore space bacterial settling times were different between the two experiments (Table **2**), but the initially high pH and bacterial movement observed indicated that they were in the active phase of the bacterial growth curve, performing ureolysis, see section 2.2. The procedure to generate calcite in the micromodel is presented in section 2.4. All experimental conditions for the two experiments are listed in Table **2**.

Table 2. Properties of bacterial- and cementation solution of experiments included in this paper.

Experiment	A	B
Properties of bacterial solution		
OD600	~0.6 *	~0.6 *
Initial pH	~ 9.2 *	~ 9.2 *
PV injected	2	2
Injection rate [µl/min]	6	6
Growth time in micromodel [h]	7	21
Temperature [°C]	31	30
Pressure [bar]	25	atm
Properties of cementation solution		
Urea [M]	1	0.5
$CaCl_2$ [M]	1	0.5
Injected [µl]	244.2	221.8
PV injected	22.0	20.0
Injection rate [µl/min]	1	1
Temperature [°C]	31	30
Initial pressure [bar]	25	atm
Pressure when pump stopped [bar]	50	10
FL included	No	Yes

* Based on measurements on three bacterial solutions made with the same procedure/volumes

During cementation solution injection (experiment A) the injection and differential pressure across the micromodel increased rapidly after 4.2 PV injected (Fig. **5**), possibly related to large amount of calcium carbonate precipitated. The PV injected increased linearly until the injection pump reached 50 bars (after 22.0 PV injected) due to blockage of the outlet tubing. Continued calcium carbonate growth was observed after injection stopped, reducing the porosity of the pore space (detailed later). For experiment B, the observed pressure behavior was similar.
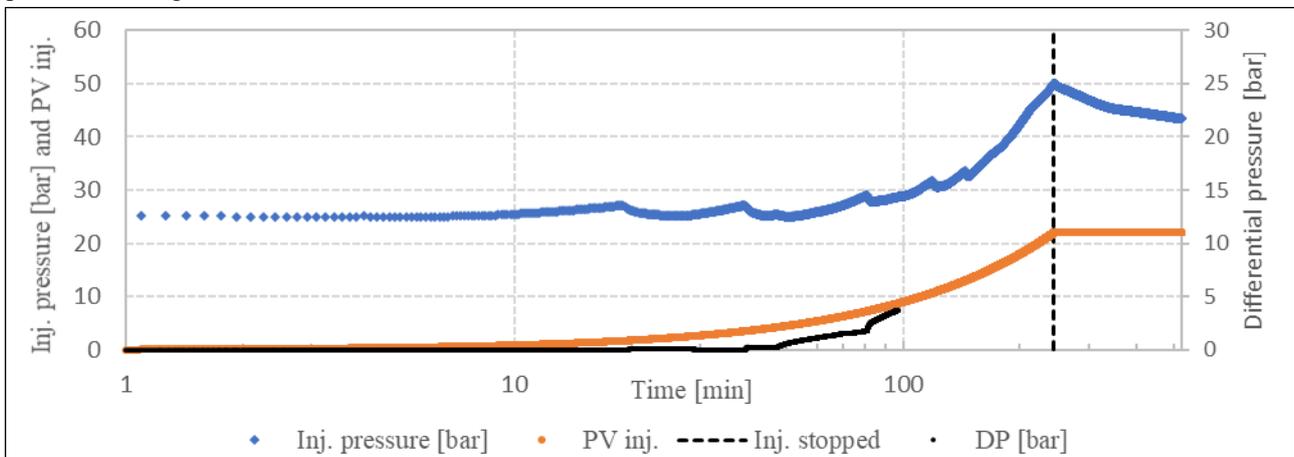
Fig. 5. Injection pressure (blue, left y-axis), differential pressure (black, right y-axis) and pore volumes injected (orange, left y-axis) during injection of cementation solution in experiment A. Injection stopped when the injection pressure reached 50 bars, indicated with vertical dashed line; measurements of differential pressure stopped at 3.7 bars because of limitation in measuring range. Calcite precipitation occurred both during injection and in a period afterwards.

3.2 Calcite precipitation

3.2.1 Single pore

The calcium carbonate grains have a variety of shapes, ranging from square/cubic, spherical to irregular (Fig. **6**). Calcite grains precipitated both close to pore walls and in the pore center, and in some cases calcite grains encapsulated silica grains. The *in-situ* development of calcium carbonate through the MICP process was further studied utilizing a fluorescence module that revealed color differences between minerals. Black calcite grains were interpreted as filling the entire height in the pores space (30 μm) and block flow. The internal structure of other minerals was visible in the FL image, in contrast to images generated with diffuser S. Hence, combining FL and diffuser S images has a large potential in characterizing the development of calcite minerals.
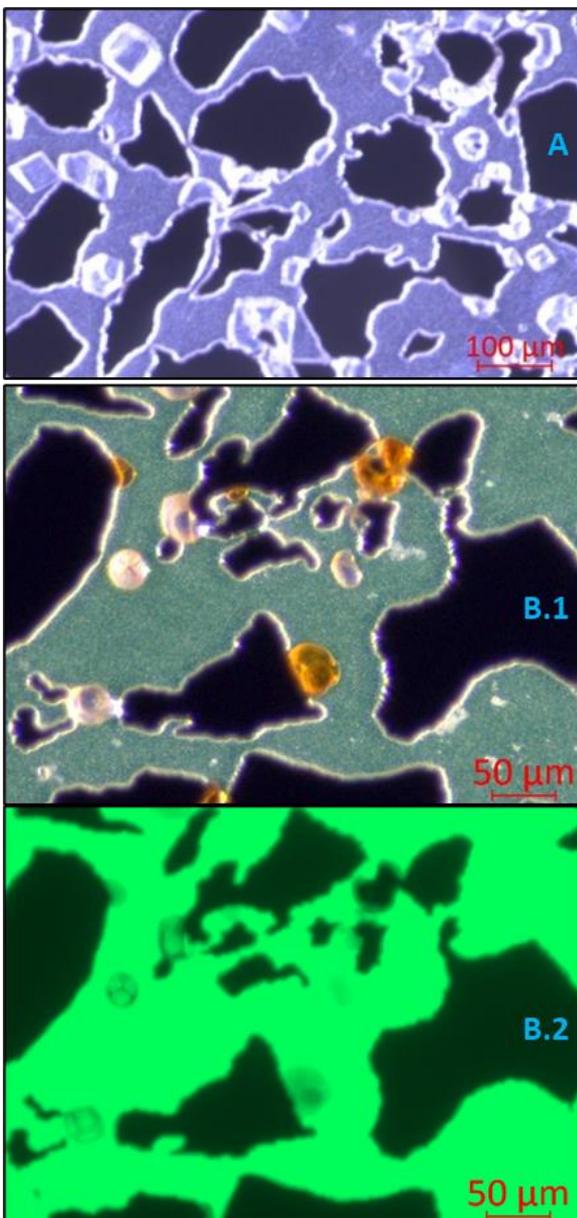
Fig. 6. Top image (A) show example of grains from experiment A, while bottom two (B) show image from experiment B generated with diffuser S light source in B.1 and with fluorescence light source in B.2.

3.2.2 Sweep/areal

The *Sporosarcina pasteurii* bacteria perform urease when settling in the micromodel, prior to injection of cementation solution. During this process, the pH is increasing and subsequently leads to carbonate ions being present in the pore space fluids. When calcium ions are added to the micromodel, calcium carbonate precipitate when the solution is supersaturated with these ions. To study the development of calcium carbonate in more detail the micromodel is divided in three subsets (Fig. **7**). The change in porosity due to calcium carbonate precipitation (Fig. **8**) was calculated using segmented images (described in section 2.5). The fraction of calcium carbonate (area of $CaCO_3$ / area of image) is summarized in Table **3**. The procedure was compared with manual measurement (using a functionality in the Zeiss software) of the total calcium carbonate grain area divided by total area in the final image (at 520 minutes) in subset 1.
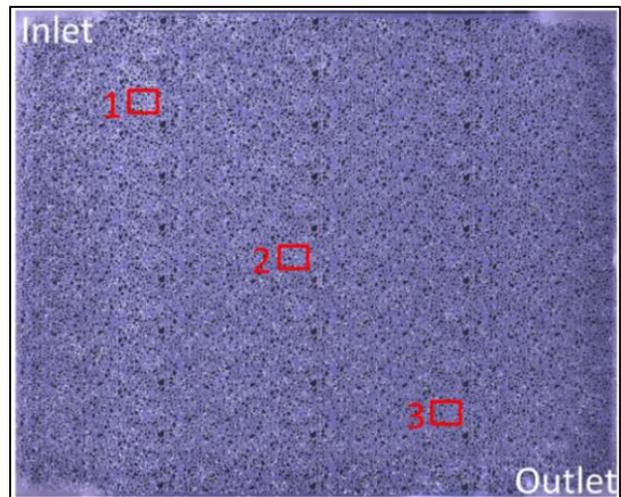
Fig. 7. Full-model image at the end of experiment A (520 min), including subset 1, 2 and 3.

Table 3. Summary of $CaCO_3$ fractions for experiment A.

Method	Area	$CaCO_3$ fraction
Polygons in Zeiss	Subset 1	0.15
Python script	Subset 1	0.13
Python script	Subset 2	0.04
Python script	Subset 3	0.02
Python script	Full-model	0.04

The development of calcium carbonate in subset 1 is detailed in Fig. **9**. Coinciding with cementation solution entering the inlet-flow-port, a small white irregularly-shaped $CaCO_3$ precipitate (< 30 μm^2) formed close to inlet and reached subset 1 after 1.4 min (0.1 PV injected). The initial porosity reduction (Fig. **8**) for subset 1 relates to these irregularly-shaped $CaCO_3$ precipitates, also seen in the image at 5 minutes in Fig. **9**. The amount of $CaCO_3$ precipitates were relatively constant until 19.3 min of injection (1.7 PV injected), when a small number of additional larger ($\sim$60-100 μm^2) irregularly-shaped $CaCO_3$ precipitates formed. Some of the irregularly-
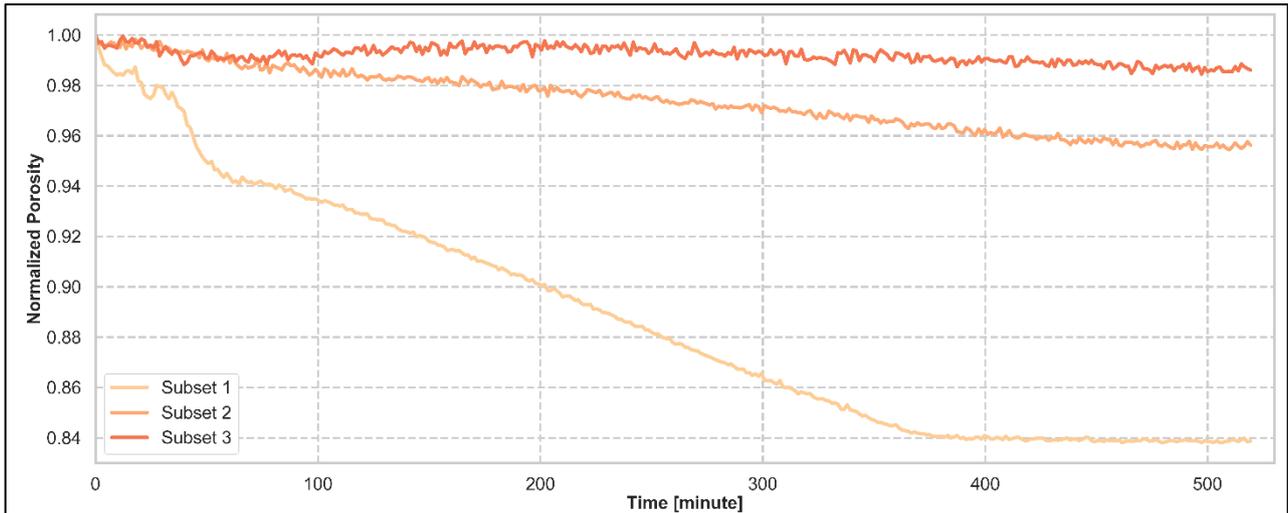
Fig. 8. Development of normalized porosity ($\Phi/\Phi_{initial}$) in each of the three subsets in experiment A. Porosity (Φ) in each timestep was calculated as: $\Phi = 1 - (areal_{silica\ grains} + areal_{CaCO_3})/total\ area$.

shaped CaCO₃ precipitates continued to grow at apparently random places in the pore space, located mainly in the middle/right side in the field of view where the pores were largest. These precipitates dissolved as
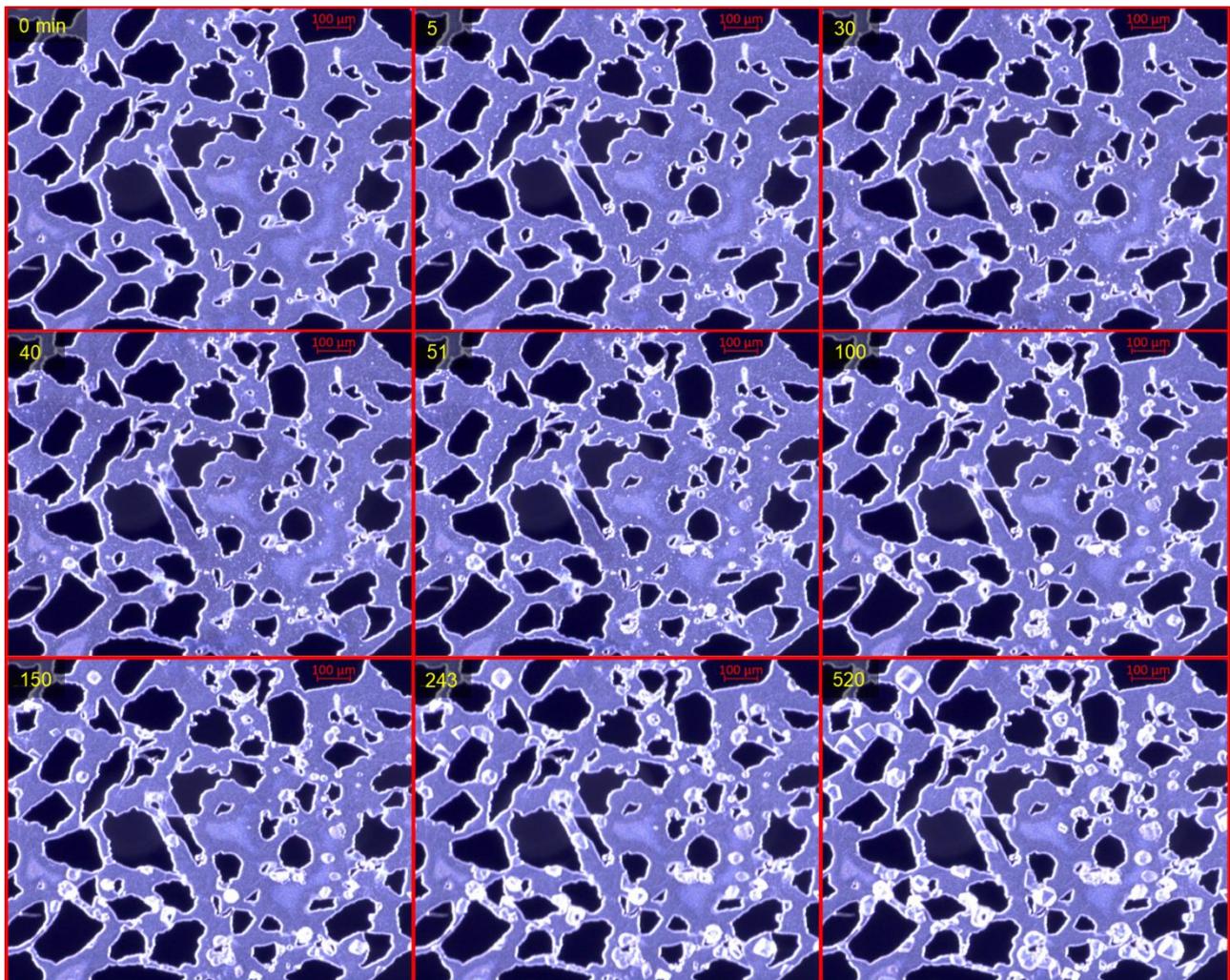
Fig. 9. Calcium carbonate precipitation in subset 1 of experiment A (Fig. 7) at different timesteps. Yellow number represent minutes from cementation solution entering the micromodel from the top left corner. This equal to PV injected until the pump stopped after 244 minutes.
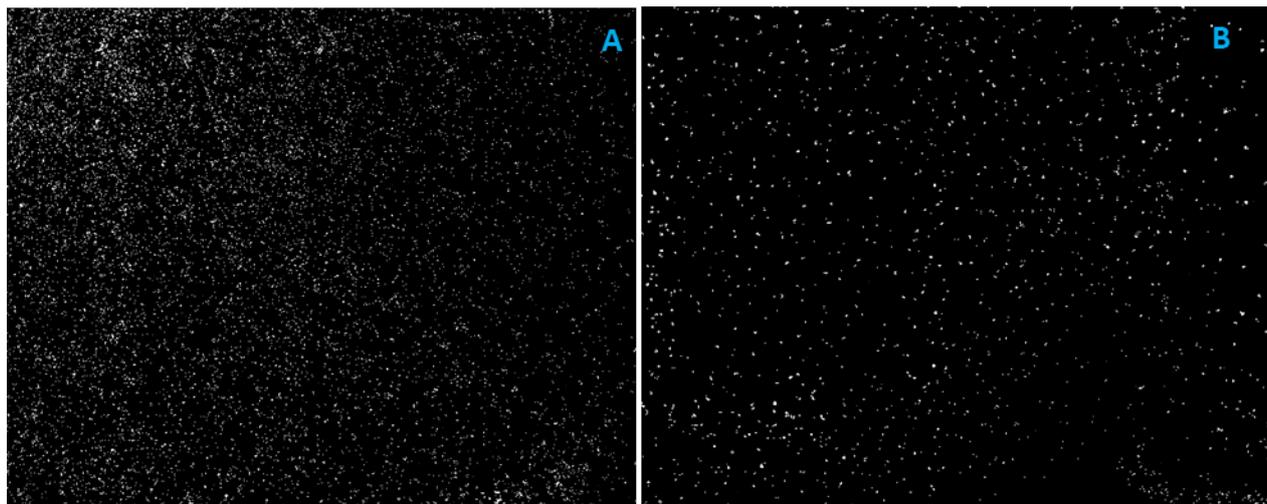
Fig. 10. Segmented images showing grains of calcium carbonate after experiment A to the left and experiment B to the right. For experiment A, the injection is at top left and outlet is bottom right, for experiment B it is opposite, with inlet at bottom right corner and outlet at top left. Width and height of both images are 24.9 mm and 19.9 mm respectively.

larger $CaCO_3$ crystals (spherical or rhombohedral) formed. These observations are consisted with findings from Wang et. al (2019) [20], reporting irregularly-shaped $CaCO_3$ dissolving in a circular trend with increasing radius outwards from the growing crystals. They further assumed that the rhombohedral crystals were calcite, spherical crystals were vaterite, and irregularly-shaped precipitates were amorphous $CaCO_3$ precipitates [20].

For the first 81 minutes, precipitating grains were predominantly spherical and/or irregularly shaped (not square or cubical). These continue to grow, but additional grains forming from this time were mainly square or cubical, with a larger area compared with the spherical grains. This change in grain precipitation coincided with a steeper slope in the differential pressure (Fig. **5**). After 244 minutes the cementation solution injection stopped (22.0 PV injected), but the calcite minerals continued to grow until 378 min. Final $CaCO_3$ fraction in subset 1 was 0.13 (Python script) or 0.15 (manual polygons drawn around all calcite minerals in the Zeiss software), confirming that the Python script could satisfactorily capture porosity reduction.

Many parameters influence the precipitation of calcium carbonate, and concentration of calcium chloride in the cementation solution is one of them. Compared to experiment A, the concentrations of calcium chloride and urea were reduced by 50% in experiment B. From the literature it is expected that lower concentration enables the cementation solution to spread out better in the pore space because the reaction is slowed down. Even though the final $CaCO_3$ fraction in subset 1 (experiment A) was 0.13, the full-model fraction was only 0.04. This indicates an uneven distribution of the carbonate minerals throughout the micromodel, and it is also visible in left section of Fig. **10**. In experiment B the full-model $CaCO_3$ fraction was calculated to 0.006, it appears to be more evenly distributed, as seen in Fig. **10**.

3.2.3   *Multiphase*

A product of bacterial respiration and urea hydrolysis is CO_2. The dissolved CO_2 form carbonic acid ($H_2O + CO_2$) and precipitates as a part of calcite (see eq 1-5), but also function as a buffer where it slows down the increasing pH as ammonia is produced by the urease [15]. At atmospheric pressure conditions some of the CO_2 develop into bubbles occupying relatively large areas in the pore volume. Because of the low injection rate, these bubbles impacted saturation distribution in the micromodel (Fig. **11**). As the permeability was reduced from precipitation of $CaCO_3$, the pore-pressure increased, and the bubble area reduced. Once a bubble was removed by dissolution in the aqueous phase, $CaCO_3$ precipitated in the area previously occupied by a bubble. It is expected that the change in pore-pressure, and hence CO_2 solubility, has an impact on the local pH value. This should be further studied by adding a pH sensitive FL tracer to the system.

3.3 Relevance to CO_2 sequestration

CO_2 sequestration in carbonate formations causes acidification of the brine and subsequent carbonate dissolution and development of reactive flow patterns. CO_2 is also a reaction product from the dissolution of calcium carbonate. Depending on the solubility and saturation of CO_2 in the pore fluid, it will go into solution or become bubbles that can eventually form a free gas phase. Song et al. 2018 presented the phenomena with a gas phase shielding carbonate minerals from dissolution as "grain engulfment" [18]. The functionalized micromodel in Experiment A was pressurized to 100 bars before CO_2 saturated HCl was injected. Fig. **12** shows CO_2 bubbles generated around $CaCO_3$ minerals during pore-level dissolution. Experiments with full model images of this dynamic reactive flow is ongoing.
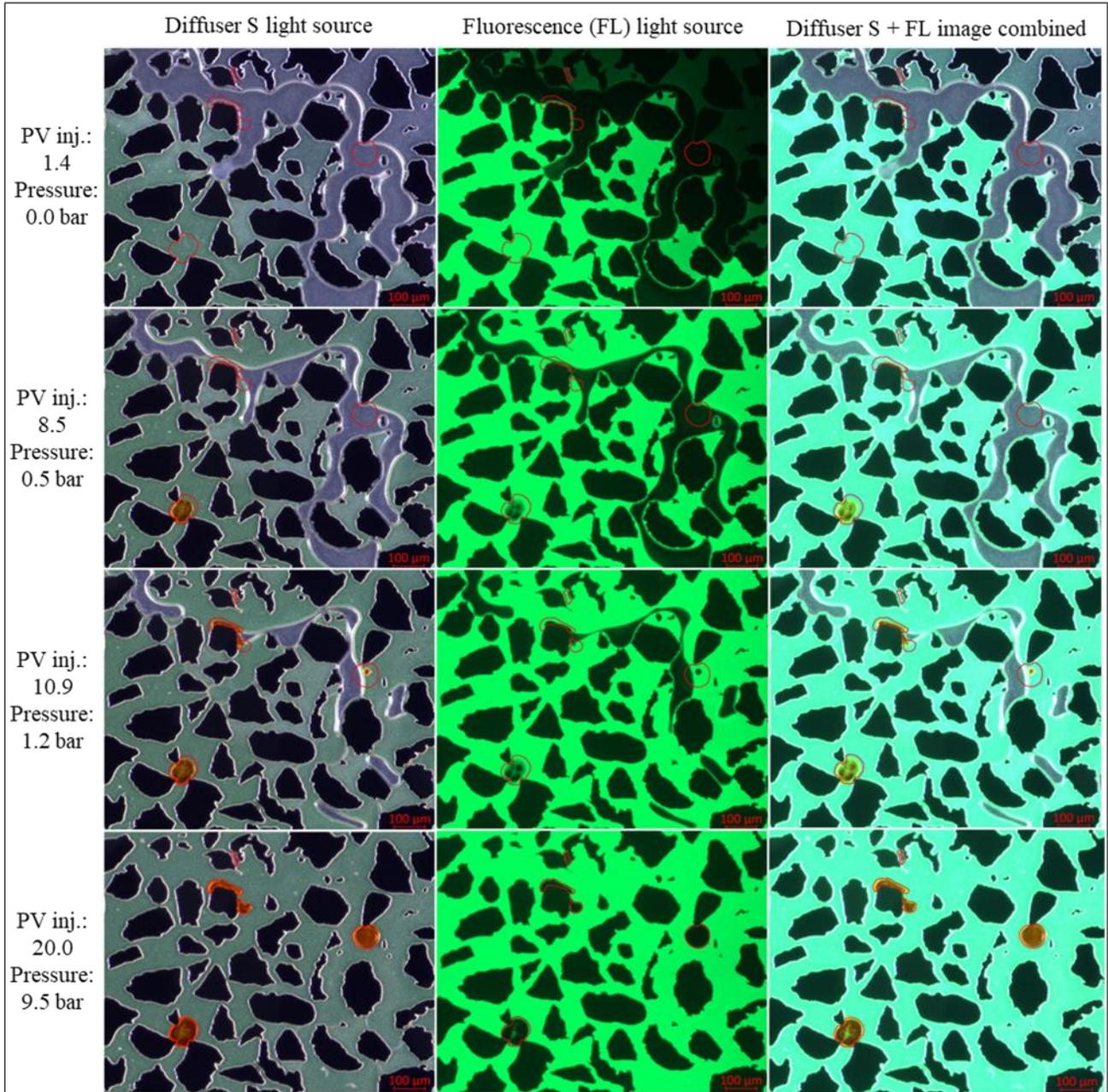
Fig. 111. Image sequence of calcium carbonate precipitation in a subset of experiment B. Pore volume injected is from cementation solution entering the micromodel in the bottom right corner (outside this field of view). Time step from top to bottom row of images are 15 min, 95 min, 122 min and 242 min, respectively. Pump stopped at 222 min (20 PV inj.). Red polygons are drawn in the Zeiss program based on image at 242 min.
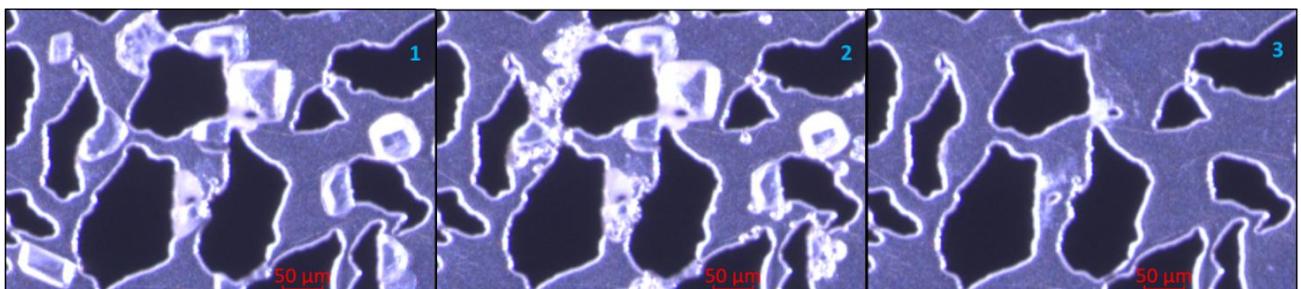
Fig. 12. Image sequence of $CaCO_3$ dissolution due to injection of CO_2 saturated HCl into a micromodel at 100 bars. Image no. 1 is from the functionalized micromodel in Experiment A, no.2 show CO_2 bubbles as the minerals dissolve and no.3 is after all the minerals have been dissolved.

4 Conclusions

Calcite-functionalization of micromodels was investigated to enable experimental investigation of fundamental pore-scale reactive transport dynamics; eventually determining carbonate CO_2 storage security. The system is very sensitive for external factors, and small procedural changes may result in large variations in results. Throughout this study we have demonstrated that bacteria are still active at 25 bar pore-pressure, and precipitation of calcium carbonate minerals occur at elevated pressures. To obtain the best conditions for segmenting of images, it is optimal to have the system under pressure and thereby limit gas-bubbles caused by the metabolism of bacteria.

This experimental set-up and methodology provide a unique method for studying the MICP process, where quantification of full-model calcite porosity development over time are demonstrated. This work also demonstrate that a micromodel can be functionalized with calcium carbonate minerals within a few days. Full-model images and elevated pressures provide the opportunity to support several research opportunities and investigations of fundamental pore-scale reactive transport dynamics:

- Carbon sequestration and dissolution of calcium carbonate
- Water weakening of chalk
- Injection rate dependency
- pH dependency using a pH sensitive FL tracer

MICP is a complex, biochemical process, and future work is planned to include a pH sensitive fluorescence tracer to improve understanding in how pH is changed throughout the different steps and how it influences the precipitation process. This focus aligns with future opportunities presented by Tang et. al (2020) [27] and would build upon work done by Zehner et.al (2020) [28] by introducing the FL tracer in a micromodel with representative pore scale geometry.

During injection of cementation solution a significant proportion of the bacteria are flushed out, as have also been reported previously [19]. This could lead to preliminary clogging of outlet tube and thereby limit amount of Ca^{2+} injected into the pore space. Future work is therefore planned with increased diameter of the outlet tube, expecting to increase calcite fraction in experiment equal to B.

Nomenclature and abbreviations

CCS	Carbon, capture and storage
CO_2	Carbon dioxide
MICP	Microbially induced calcite precipitation
BHI	Brain Heart Infusion
BHI+U	Brain Heart Infusion including urea
DI	Deionized water
OD600	Optical density measured at a wavelength of 600 nm
PEEK	Polyether ether ketone
$CaCO_3$	Calcium carbonate
$CO(NH_2)_2$	Urea
$CaCl_2$	Calcium chloride
NH_3	Ammonia
NH_4^+	Ammonium
H_2CO_3	Carbonic acid
HCO_3^-	Bicarbonate
CO_3^{2-}	Carbonate ions
Ca^{2+}	Calcium ions
FL	Fluorescent
Φ	Porosity
HCl	Hydrochloric acid
H_2O	Water

References

1. IEA, *The Role of CO2 Storage.* (2019).
2. W. De Muynck, N. De Belie, and W. Verstraete, *Microbial carbonate precipitation in construction materials: A review,* Ecological Engineering, **36**(2): p. 118-136 (2010)
3. F.G. Ferris, et al., *Bacteriogenic Mineral Plugging,* Journal of Canadian Petroleum Technology, **36**(09): p. 5 (1996)
4. J. Wu, et al., *Microbially induced calcium carbonate precipitation driven by ureolysis to enhance oil recovery,* RSC Advances, **7**(59): p. 37382-37391 (2017)
5. Y. Fujita, et al., *Evaluating the Potential of Native Ureolytic Microbes To Remediate a 90Sr Contaminated Environment,* Environmental Science & Technology, **44**(19): p. 7652-7658. (2010)
6. F.D. Meyer, et al., *Microbiologically-Induced Soil Stabilization: Application of Sporosarcina pasteurii for Fugitive Dust Control*, Geo-Frontiers, Vol. 2011, p.4002-4011 (2011)
7. A.C. Mitchell, et al., *Microbially Enhanced Carbon Capture and Storage by Mineral-Trapping and Solubility-Trapping.* Environmental Science & Technology, **44**(13): p. 5270-5276 (2010)
8. A. Phillips, et al., *Potential CO2 Leakage Reduction through Biofilm-Induced Calcium Carbonate Precipitation,* Environmental Science & Technology, **47**: p. 142-149 (2013)
9. A.B. Cunningham, et al., *Microbially enhanced geologic containment of sequestered*

supercritical CO2, Energy Procedia, **1**(1): p. 3245-3252 (2009)

10. F. Hammes, and W. Verstraete*, *Key roles of pH and calcium metabolism in microbial carbonate precipitation.* Reviews in Environmental Science and Biotechnology, **1**(1): p. 3-7 (2002)

11. B. Krajewska, *Urease-aided calcium carbonate mineralization for engineering applications: A review.* Journal of Advanced Research, **13**: p. 59-67 (2018)

12. J.W. Mullin, *Crystallization*, 4th ed., Oxford: Butterworth-Heinemann (2001)

13. W. Zhang, et al., *In Situ Real-Time Study on Dynamics of Microbially Induced Calcium Carbonate Precipitation at a Single-Cell Level,* Environmental Science & Technology, **52**(16): p. 9266-9276 (2018)

14. L.A. Van Paassen, *Biogrout, ground improvement by microbial induced carbonate precipitation*, in *TU Delft, Applied Sciences*, TU Delft: The Netherlands (2009)

15. S. Stocks-Fischer, J.K. Galinat, and S.S. Bang, *Microbiological precipitation of CaCO3.* Soil Biology and Biochemistry, **31**(11): p. 1563-1571 (1999)

16. G.E. Mountassir, et al., *Hydrodynamic coupling in microbially mediated fracture mineralization: Formation of self-organized groundwater flow channels,* Water Resources Research, **50**(1): p. 1-16 (2014)

17. C. Wu, et al., *Microbially induced calcite precipitation along a circular flow channel under a constant flow condition,* Acta Geotechnica, **14**(3): p. 673-683 (2019)

18. W. Song, et al., *Mechanisms of Multiphase Reactive Flow using Biogenically Calcite-Functionalized Micromodels,* Lab on a Chip, **18**, (2018)

19. Y. Wang, et al., *A microfluidic chip and its use in characterising the particle-scale behaviour of Microbial-Induced Carbonate Precipitation (MICP),* Géotechnique, **69** (2018)

20. Y. Wang, et al., *Microscale Visualization of Microbial-Induced Calcium Carbonate Precipitation Processes,* Journal of Geotechnical and Geoenvironmental Engineering, **145**: p. 04019045 (2019)

21. M. Buchgraber, et al., *Creation of a dual-porosity micromodel for pore-level visualization of multiphase flow,* Journal of Petroleum Science and Engineering, **86-87**: p. 27-38 (2012)

22. M. Buchgraber, A.R. Kovscek, and L.M. Castanier, *A Study of Microscale Gas Trapping Using Etched Silicon Micromodels,* Transport in Porous Media, **95**(3): p. 647-668 (2012)

23. B. Benali, et al. *[Preprint] Pore-scale Bubble Population Dynamics of CO2-Foam at Reservoir Pressure.* https://essoar.org (2021)

24. J.H. Yoon, et al., *Sporosarcina aquimarina sp. nov., a bacterium isolated from seawater in Korea, and transfer of Bacillus globisporus (Larkin and Stokes 1967), Bacillus psychrophilus (Nakamura 1984) and Bacillus pasteurii (Chester 1898) to the genus Sporosarcina as Sporosarcina globispora comb. nov., Sporosarcina psychrophila comb. nov. and Sporosarcina pasteurii comb. nov., and emended description of th.* International Journal of Systematic and Evolutionary Microbiology, **51**(3): p. 1079-1086 (2001)

25. P. De Vos, G.M. Garrity, and D.H. Bergey, *Bergey's manual of systematic bacteriology: Vol. 3 : The Firmicutes.* 2nd ed. Vol. 3., New York: Springer (2009)

26. M.S. Reddy, *Biomineralization of calcium carbonates and their engineered applications: a review,* Frontiers in Microbiology, **4**(314) (2013)

27. C.-S. Tang, et al., *Factors affecting the performance of microbial-induced carbonate precipitation (MICP) treated soil: a review.* Environmental Earth Sciences, **79**(5): p. 94 (2020)

28. J. Zehner, et al., *Microbial-induced calcium carbonate precipitation: an experimental toolbox for in situ and real time investigation of micro-scale pH evolution,* RSC Advances, **10**(35): p. 20485-20493 (2020)